Numerical Investigation of Pressure Pulsation in Oil-Free Twin Screw Compressor Discharge Systems Adopted to Oil and Gas Industry

Vitor Braga*, Ernane Silva, Thiago Dutra, Andre Caetano, Olavo Silva, Arthur Andreazza
Federal University of Santa Catarina
Florianopolis, SC, Brazil
vitor.braga@polo.ufsc.br, ernane.silva@teg.ufsc.br, thiago.dutra@teg.ufsc.br, caetano@mopt.ufsc.br, olavo@lva.ufsc.br, arthur.andreazza@teg.ufsc.br

* Corresponding Author

ABSTRACT

Pressure pulsation within the discharge system of oil-free twin-screw compressors used in Vapor Recovery Units (VRUs) significantly impacts their reliability and the integrity of connected piping. This study investigates the dynamics of pressure pulsations in such compressors within the oil and gas industry, where reliable and robust operation is crucial. A Computational Fluid Dynamics (CFD) model was developed using ANSYS CFX coupled with SCORG mesh generation. Different discharge system configurations were investigated, including scenarios with the discharge port only, discharge port with a venturi pipe and a discharge port with a constant diameter pipe. Non-Reflective Boundary Conditions (NRBC) were adopted at the discharge outlet to minimize wave reflection. Findings revealed minor variations in both the P-α diagram and pulsation profiles among the configurations. Specifically, the use of a venturi pipe slightly elevated the peak pressure in the P-α diagram and increased the amplitude of discharge pressure pulsations. Additionally, the mass flow rate and indicated power showed negligible variation across the configurations, highlighting the limited impact of discharge system design on these performance metrics. Finally, a frequency domain analysis revealed the presence of the pocket passing frequency and no resonance effects due to different discharge configurations.

1. INTRODUCTION

Screw compressors are widely used in different industries that demand large flow rates of compressed gas. As positive displacement machines, a pulsating flow is delivered at the discharge port of these compressors, which may cause failure of system components if it is not properly damped. These pressure pulsations are intensified at off design conditions when under-compression or over-compression occurs, reaching as much as 10-20 percent of the absolute discharge pressure (Huang, 2018). Zhao et al. (2019), for instance, describe excessive vibration induced by pulsation in the outlet piping system as one of the main causes of premature failure of thermowells and unplanned shutdowns of a screw compressor used in a chemical plant. A similar condition is found in Vapor Recovery Units (VRUs) employed to capture volatile compounds in oil and gas operations.

Different strategies have been used to predict discharge pressure pulsations within screw compressors. Mujic et al. (2008) adopted a numerical model based on the mass and energy conservation principles to evaluate the pressure pulsation levels in the discharge chamber of an oil-flooded air compressor. The analysis indicated that the most influential parameters affecting gas pulsations were the pressure difference between the compressor working and discharge chambers and the discharge port area. The authors proposed the optimization of the port shape to reduce its amplitude. Chen et al. (2019) developed a similar model for a twin-screw refrigeration compressor which was validated against experimental data. The model was then applied to investigate the effects of operational and design parameters on the discharge pressure pulsations, providing valuable information for compressor design and optimization.

Mujic et al. (2009) compared the accuracy and computational time of three different models used to predict the pressure pulsation in the discharge chamber: one dimensional flow (Mujic et al., 2008), three-dimensional flow, and a combination of the two. The three-dimensional flow in the whole compressor domain, including suction, working,

and discharge chambers, was solved using the CFD commercial solver Comet. The coupled model combines the one-dimensional flow simulation in the suction and working chambers with the three-dimensional flow simulation in the discharge chamber. The authors pointed out that the one-dimensional model has the shortest running time but is only adequate for the prediction of the first harmonic. When higher accuracy is required, the three-dimensional flow model should be adopted at the expense of a longer running time. A negligible loss of accuracy is observed in the coupled model with a one order of magnitude lower computational effort.

Three dimensional CFD simulations have become more usual for screw compressor analysis and design with the continuous increase of computational power and software capabilities, especially for mesh generation. For instance, Pascu et al. (2013) evaluated the influence of the suction port arrangement of a twin-screw air compressor on performance. Yang et al. (2021) studied the pressure pulsations inside the working chamber of an oil-injected twin-screw refrigeration compressor.

Several studies in the literature also deal with the propagation of the pressure pulsations through the discharge piping system and the analysis of solutions to mitigate its effect. The present study analyzes the pressure pulsations in the discharge port of oil-free twin-screw compressors used in Vapor Recovery Units (VRUs). A three-dimensional CFD model is developed and the influence of the outlet domain on the pressure pulsation is evaluated.

2. NUMERICAL MODEL

For the Computational Fluid Dynamics (CFD) simulation of the screw compressor described in this work, Ansys CFX 2023 R2 was utilized in conjunction with SCORG, the latter being employed for the computational mesh generation of the rotors. The chosen compressor model for analysis operates oil-free, has rotor diameters of 321.3 mm and a length of 530.1 mm (L/D = 1.65). The male rotor has 4 lobes, and the female rotor has 6 lobes (4/6 configuration). The volume index is 2.69.

Three configurations of the discharge system were explored to assess their influence on the pressure pulsations: discharge port only (A), discharge port with constant diameter pipe (B) and discharge port with a venturi pipe (C), as illustrated in Figure 1. For all setups, the discharge port has an outlet diameter of 292 mm and a volume of 0.013 m³. In configuration B, the discharge pipe measures 292 mm in diameter and is 750 mm long, resulting in a volume of 0.05 m³. Finally, configuration C incorporates a venturi pipe with a maximum diameter of 436 mm, a minimum diameter of 192 mm, an overall length of 1.8 m, and a total volume of 0.144 m³.

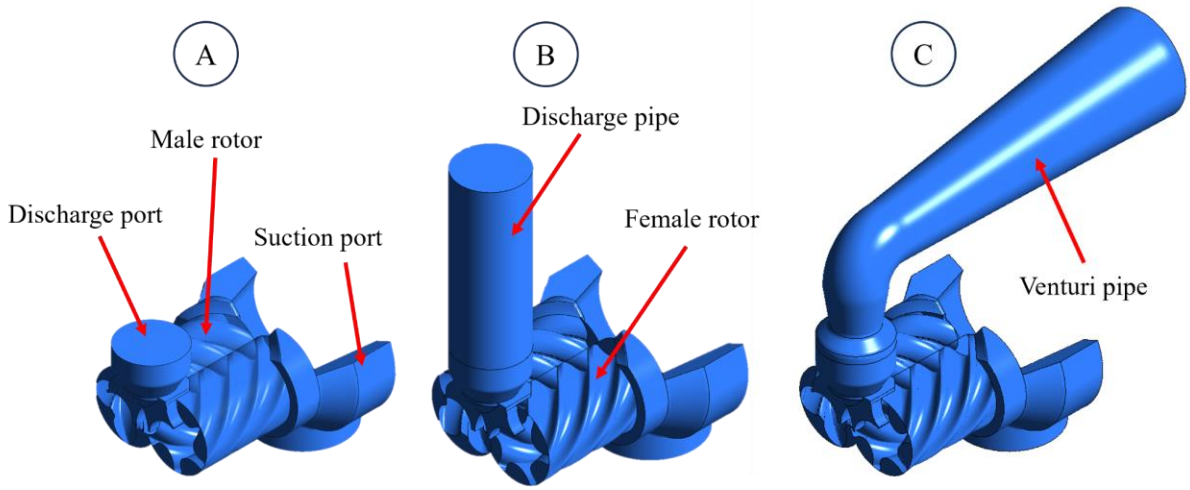

Figure 1. Discharge system configurations: discharge port only (A), discharge port with constant diameter pipe (B), discharge port with venturi pipe (C).

2.1 Computational model setup

The simulations are carried out with an unsteady approach, constrained to 10 full rotations of the main shaft, equivalent to 2400 time steps, with each time step representing a 1.5-degree rotation, determined by the mesh generated in SCORG. The time increment is calculated based on the mesh and the rotational speed of the compressor, resulting in approximately 47.2 microseconds. The adopted turbulence model is the Shear Stress Transport (SST) k-ω with wall functions. Second-order schemes are employed for the calculation of pressure, velocity, and temperature, and a first-order scheme is utilized for the variables of the turbulence model and time discretization. Relaxation factors for velocity, pressure, and temperature are set at 0.05 to ensure numerical stability. The working fluid employed in the simulations consists of a mixture of hydrocarbons, resulting in the properties listed in Table 1.

Table 1. Working fluid properties.

Property	Value
Molar mass	44.87 kg/kmol
Specific heat at constant pressure	1724 J/(kg.K)
Viscosity	10.2 μPa.s
Density	Ideal gas EoS
Thermal conductivity	25.3 mW/(m.K)

The simulation's boundary conditions, specified in Table 2, include a Non-Reflective Boundary Condition (NRBC) at the discharge outlet to minimize wave reflection, with a reflection factor of 0.25, reflection Mach scale of 0.2 and a reflection length scale equivalent to the length of the considered discharge system. The use of NRBC is fundamental for the configurations B and C (see Figure 1) to avoid highly oscillatory behavior. Without NRBC, parameters such as discharge pressure and mass flow rate would exhibit significant oscillations, preventing the attainment of a fully developed cyclic regime in the screw compressor.

For the dynamic mesh associated with the rotors, we employ a user-defined nodal displacement grid deformation method, following Kovacevic et al. (2007). This method is the most appropriate for screw compressor simulations, according to Rane et al. (2013).

Table 2. Boundary conditions.

Location	Boundary type	Value
Suction inlet	Opening	P = 2.0 bar (abs), T = 305 K
Discharge outlet	Opening with NRBC	P = 7.7 bar (abs)
Rotors	Moving wall	N = 5296 rpm

For the configuration featuring only the discharge port (A), all domains are initialized from the compressor suction conditions. Then, the results for the rotors and the suction port serve as the initial conditions for subsequent configurations (B and C). Given the substantial pressure difference between the suction and discharge boundaries, a pressure ramp increases the discharge outlet pressure from 2.0 bar to 7.7 bar over 200 time steps.

The simulation is considered converged when the pressure profile monitored along the male rotor stabilizes, indicating a fully developed cyclic regime. This state was typically reached after about 10 days on a workstation equipped with an AMD Ryzen 9 5950X 16-Core 3.40 GHz processor and 128 GB RAM.

2.2 Computational mesh generation and mesh independence study

The rotor mesh is created with SCORG, using the SRM-A profile generated by an in-house code. To verify the mesh effect on the results, two mesh sizes were tested: a coarse mesh with 91 circumferential, 13 radial, and 60 angular divisions; and a refined mesh with 132, 19, and 60 divisions, respectively. Both meshes maintain a 0.23 mm clearance for all gaps. The suction and discharge ports, along with the discharge pipe (for configurations B and C), have grids generated by Ansys Workbench Meshing. The coarse mesh contains around 4 million elements, while the refined mesh holds approximately 8.8 million.

Table 3 displays results from both meshes for configuration B, indicating that the coarse mesh accurately predicts the compressor indicated power and mass flow rate. Furthermore, Figure 2 demonstrates that the pressure within the compression chamber as a function of the main shaft angle (P-α diagram) and the discharge pressure are consistent across both meshes. Therefore, the coarse mesh is used for the analyses in this study.

Table 3. Comparison of the results from the coarse and refined meshes.

Parameter	Coarse mesh	Refined mesh	Difference [%]
Mass flow rate [kg/h]	27112	27132	0.07%
Indicated power [kW]	752	751	0.22%

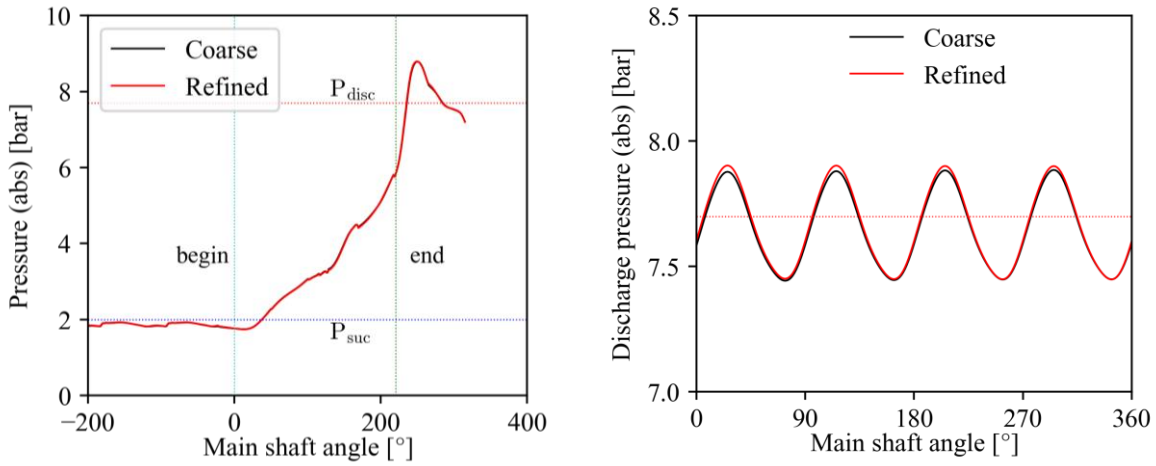

(a) (b)

Figure 2. Comparison of the results from the coarse and refined meshes: (a) P-α diagram, (b) discharge pressure. The vertical dotted lines represent the beginning and end of compression, while the horizontal dotted lines indicate the discharge pressure (P_{disc}) and the suction pressure (P_{suc}).

3. RESULTS

Figure 3 illustrates the P-α diagrams for the different discharge system configurations. Configurations A and B yield nearly identical pressure profiles, indicating that a constant diameter tube has minimal effect on the pressure within the rotors. However, configuration C shows a notable deviation, with a higher-pressure peak after the end of the compression process, aligning with expectations due to the venturi tube's flow restriction, which necessitates an increased discharge pressure to compensate for the head loss.

To compute the compressor discharge pressure, we average the absolute pressure over the area highlighted in yellow in Figure 4. For configuration A, the yellow surface is the domain outlet, while for B and C, it represents the interface between the discharge port and pipe. Figure 5 shows the pressure pulsations at the compressor discharge, reaffirming the Figure 3 findings, A and B are consistent with each other, but C showcases a higher pulsation amplitude in discharge pressure. Nonetheless, the mean discharge pressure across all configurations closely matches the set boundary condition of 7.7 bar, as depicted by the dotted line.

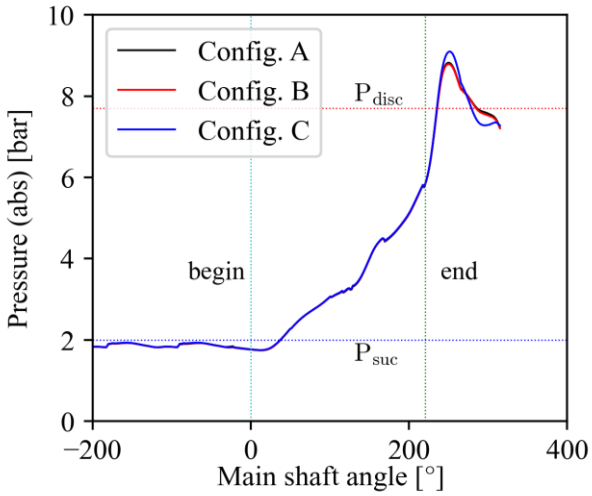

Figure 3. P-α diagram for the three discharge geometry configurations.

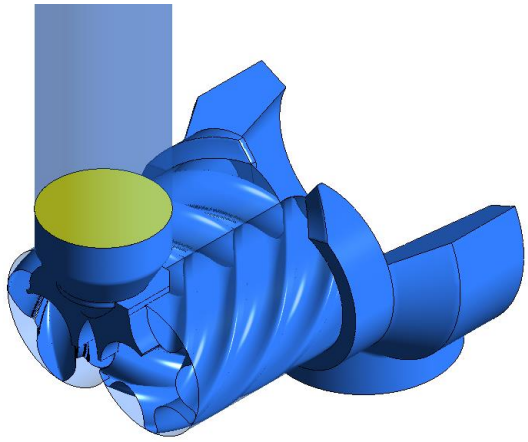

Figure 4. Surface used for the discharge pressure calculation (highlighted in yellow).

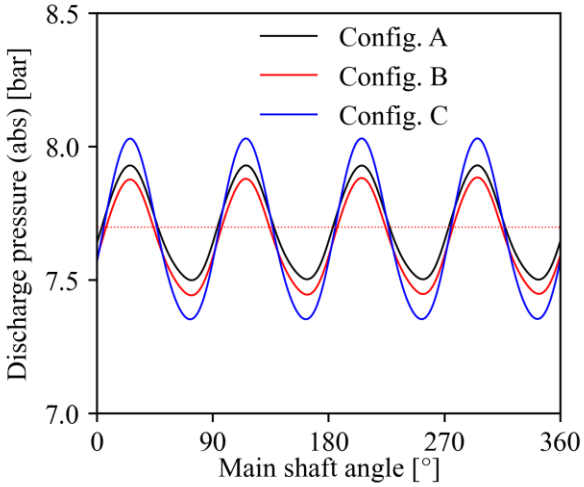

Figure 5. Discharge pressure for the three discharge geometry configurations.

Table 4 compares the mass flow rate and indicated power for the configurations, demonstrating negligible differences between them. The largest variance is in configuration C's indicated power, a less than 1% increase compared to the others. This slight rise corresponds with the P-α diagram observed in Figure 3 and aligns with the computation of indicated power, which is derived from the internal rotor pressures.

Table 4. Mass flow rate and indicated power obtained from the three configurations.

Parameter	Configuration A	Configuration B	Configuration C
Mass flow rate [kg/h]	27192	27112	27130
Indicated power [kW]	753	752	759

When analyzed in the frequency domain, the pulsations at the compressor discharge reveal crucial insights into the behavior of boundary conditions and operational conditions of the system. The primary goal of non-reflective boundary conditions is to represent an anechoic acoustic field, thereby minimizing the effects of resonances associated with the truncation of the discharge pipe length. Figure 6 illustrates the frequency spectra of the pulsations for different configurations. The dominant frequency of 353 Hz remains identical across all cases, consistent with the system's pocket passing frequency, indicating no resonance effects associated with varying geometries. However, there is a significant difference in the amplitudes of configuration C compared to the others, corroborating the findings observed in the time domain.

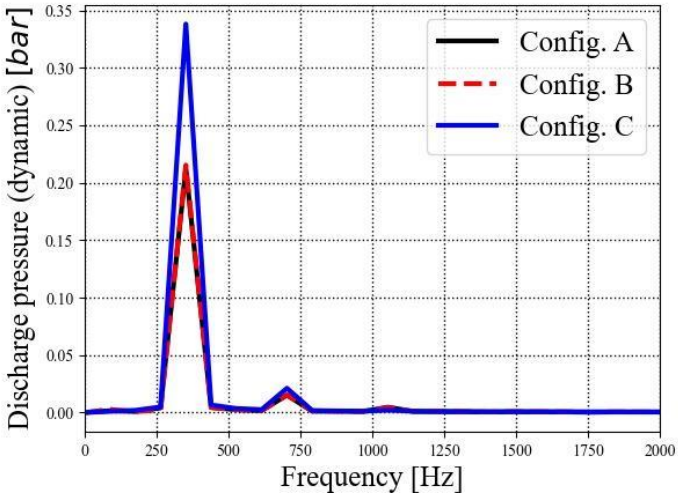

Figure 6. Frequency spectrum of discharge pressure pulsations for the three discharge geometry configurations.

3.1 Reflection factor sensitivity analysis

The reflection factor (σ) is a key parameter in defining the Non-Reflective Boundary Conditions (NRBCs) used in this study. An ideal non-reflective condition requires $\sigma = 0$, but this leads to numerical instability. Consequently, larger σ values are employed, with higher values resulting in a higher cutoff frequency for waves reflected at the boundary. As σ increases, the boundary gradually approaches a fully reflective condition.

To further investigate its impact, additional simulations were conducted with configuration B, using alternative reflection factor values of $\sigma = 1$ and $\sigma = 2$, in addition to the default value of $\sigma = 0.25$ proposed by Poinsot and Lele (1992). The effects of these modified reflection factors on the P-α diagram and pressure pulsation at the compressor discharge were subsequently analyzed.

The results for the P-α diagram, illustrated in Figure 7, reveal significant differences during the discharge process. Notably, the pressure profile remains smooth with minimal oscillations when σ = 0.25. In contrast, increasing the reflection factor to σ = 1 and σ = 2 yields a higher pressure peak, accompanied by the emergence of additional pressure oscillations. A similar trend is observed in Figure 8, which displays the pressure pulsation at the discharge. Here, the smooth pressure profile obtained with σ = 0.25 is disrupted by the introduction of overlapping oscillations and increased pressure amplitude when σ = 1 and σ = 2 are employed.

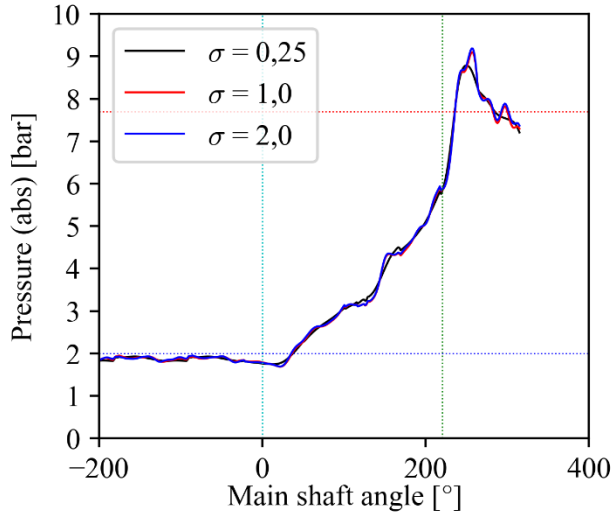

Figure 7. P-α diagram for the different values of reflection factor (σ).

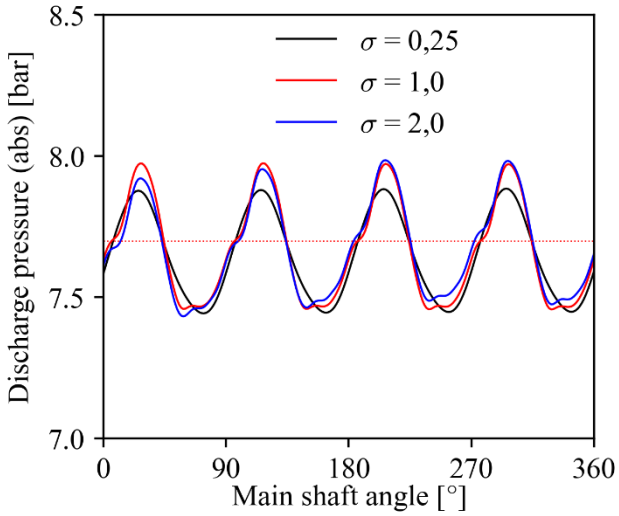

Figure 8. Discharge pressure for the different values of reflection factor (σ).

4. CONCLUSIONS

This paper reported the development of a CFD model to investigate the rotor internal pressure profile (P-α diagram) and discharge pressure pulsations in an oil-free twin-screw compressor, used in Vapor Recovery Units (VRUs). Three configurations of discharge systems were examined: discharge port only (A), discharge port with constant diameter pipe (B) and discharge port with a venturi pipe (C). Non-Reflective Boundary Conditions (NRBC) were integrated into the model to mitigate wave reflections at the domain outlet.

Findings revealed minor variations in both the P-α diagram and pulsation profiles among the configurations. Specifically, the use of a venturi pipe in configuration C slightly elevated the peak pressure in the P-α diagram and increased the amplitude of discharge pressure pulsations. Nevertheless, the mean discharge pressure for all configurations was consistent with the boundary condition value of 7.7 bar. Additionally, the mass flow rate and indicated power showed negligible variation across the configurations, highlighting the limited impact of discharge system design on these performance metrics. A frequency domain analysis revealed the presence of the pocket passing frequency and no resonance effects due to different discharge configurations. Finally, the reflection factor is shown to have a substantial impact on both the internal rotor pressure and discharge pressure pulsations, altering not only the pulsation amplitude but also introducing additional oscillation components. Therefore, these findings emphasize the need for experimental validation to ensure the accuracy of numerical simulations.

REFERENCES

Chen, W., Wu, X., Xing, Z., & Wang, X. (2019). Investigation of characteristics of discharge pressure pulsation in a twin-screw refrigeration compressor. *Proceedings of the Institution of Mechanical Engineers, Part C: Journal of Mechanical Engineering Science, 233(6*), 2206-2224.

Huang, P. X. (2018). A model for the transient pulsation generation at the discharge of a screw compressor by a shock tube analogy. *In IOP Conference Series: Materials Science and Engineering* (Vol. 425, No. 1, p. 012022). IOP Publishing.

Koai K and Soedel W. (1990) Gas pulsation in screw compressors– part 1: determination of port flow and interpretation of periodic volume source. *In: Proc. 10th International Compressor Engineering Conference at Purdue*, USA, pp.369–377.

Koai K and Soedel W. (1990) Gas pulsation in screw compressors– part 2: dynamics of discharge system and its interaction with port flow. *In: Proc. 10th International Compressor Engineering Conference at Purdue*, USA, pp.378–387.

Kovacevic, A., Stosic, N., & Smith, I. (2007). *Screw Compressors: Three Dimensional Computational Fluid Dynamics and Solid Fluid Interaction*. New York, NY: Springer.

Mujic, E., Kovacevic, A., Stosic, N., & Smith, I. K. (2008). The influence of port shape on gas pulsations in a screw compressor discharge chamber. *Proceedings of the Institution of Mechanical Engineers, Part E: Journal of Process Mechanical Engineering, 222(4)*, 211-223.

Mujić, E., Kovačević, A., Stošić, N., & Smith, I. K. (2009) Numerical modelling of gas pulsations in a screw compressor. Institution of Mechanical Engineers - *International Conference on Compressors and their Systems*, pp 33-40.

Pascu, M., Heiyanthuduwage, M., & Mounoury, S. (2013). Influence of the suction arrangement and geometry of the inlet port on the performance of twin screw compressors. *In 8th Int. Conf. Compress. their Syst.*

Poinsot, T. J., Lele, S. K. (1992). Boundary conditions for direct simulations of compressible viscous flows. *Journal of Computational Physics, 101*, 104-129.

Rane, S., Kovacevic, A., Stosic, N., & Kethidi, M. (2013). Grid deformation strategies for CFD analysis of screw compressors. *International Journal of Refrigeration, 36*, 1883-1893.

Wu, H., Xing, Z., Peng, X., & Shu, P. (2004). Simulation of discharge pressure pulsation within twin screw compressors. *Proceedings of the Institution of Mechanical Engineers, Part A: Journal of Power and Energy*, 218(4), 257-264.

Yang, S., Ouyang, H., Wu, Y., Wang, L., Mei, L., & Wang, H. (2021). CFD simulation for the internal pressure characteristics of an oil-injected twin-screw refrigeration compressor. *International Journal of Refrigeration, 126*, 143-154.

Zhao, Y., Feng, J., Zhao, B., Zhou, S., Tang, Z., & Peng, X. (2019). Vibration analysis and control of a screw compressor outlet piping system. *Proceedings of the Institution of Mechanical Engineers, Part E: Journal of Process Mechanical Engineering, 233(2)*, 403-411.

ACKNOWLEDGEMENT

Financial support from PETROBRAS SA (Grant 2022/00268-2) is acknowledged.